2011 50th IEEE Conference on Decision and Control and
European Control Conference (CDC-ECC)
Orlando, FL, USA, December 12-15, 2011

Formation control of fully-actuated marine vessels using group agreement protocols

Christoffer F. L. Thorvaldsen and Roger Skjetne

Abstract— **This paper addresses the problem of getting fully-actuated marine surface vessels to establish a formation before executing its mission, which here is to traverse a predetermined path. Whereas existing designs typically solve the problem by establishing the formation on the path, the proposed design in this paper allows the vessels to coordinate at an arbitrary location prior to a collective movement to the path. Protocols for group agreement form the basis of the proposed solution, while ideas from maneuvering control theory are incorporated to yield the desired path-following behavior. To demonstrate the design, a simulation is shown, where the formation's capability of handling a severe single vessel failure is illustrated.**

I. Introduction

As an area of research, formation control has attracted increasing effort in recent times. Although the specific applications have been diverse, ranging from survey-missions on the ocean surface to cooperative control of satellites in space, the research efforts share the desire to use formations to enable execution of complex operations that are infeasible or less efficient for single agents. In the marine domain, possible applications of formation control include operations such as underway replenishment, towing of structures, geological surveying, unmanned scouting, and fleet transit. In the future it is also envisioned formations of unmanned ships for efficient transport of cargo.

Many designs for formation control exists in the literature, providing solutions for different classes of dynamical systems and different formation objectives. Examples are the general designs in [2], [9], [10], [11] and [13], the designs for mobile robots in [12] and [14], and the design for spacecraft in [15]. Within the marine control community, a large amount of work has been done within a path-based framework, where one wants the formation to move along a prespecified path with a desired speed. Examples are the formation maneuvering design in [4], the extensions provided in [5], and the guided leader-follower approach in [6].

A common trait in these designs is that the formation is established by controlling the individual vessels to their correct positions relative to a point on the path. When the formation is established, the formation as a whole is already positioned on the path, meaning that the task of coordinating the vessels is entwined with the path-following operation. The idea pursued herein is to provide a design that enables a separation between the tasks of group coordination and the path-following mission. The vessels will then primarily establish a formation in the vicinity of their present location. Secondarily, a collective path-following operation is initiated when the vessels are sufficiently coordinated. By making sure that the vessels are safely coordinated before convergence to the path is attempted, the danger of collisions during the transient motion towards the path is alleviated. Additionally, in regard to an operational philosophy where the formation should be maintained at all costs, robustness to severe vessel failures such as blackouts followed by drift-off of a single vessel, is also achieved.

The basis of our design is the passivity-based group coordination framework in [2]. Generically, the framework can be used to coordinate output variables of dynamical systems in a decentralized manner while achieving a specified, common velocity in the limit for all the outputs. In [2] the common velocity signal is assumed to be known and available for each system, whereas in [9] this is extended by an adaptive scheme where all but one of the systems estimate the velocity. An application towards formation control is given, where the output variables are coordinated according to a formation constraint function. The presence of local minima in the example design in [2], however, has motivated the use of another approach to achieve coordination. Establishing the desired formation structure will be formulated as a synchronization problem involving agreement of coordination variables across the group of vessels.

With respect to the common categorization of formation control designs into behavioral, leader-follower, and virtual structure schemes, the design proposed herein shares common traits with the decentralized virtual structure (DVS) approach presented in [16]. The DVS approach formulates the group coordination problem (partly) as a synchronization problem where the coordination variables corresponds to the states of local virtual structures that produce reference signals for their corresponding agents to track. Whereas DVS tries to achieve synchronization of the coordination variables while simultaneously attempting convergence of these variables to a common set-point, the coordination approach taken herein allows for the formation to stabilize at an arbitrary location prior to pursuing the formation mission objective.

A. Main contributions

Providing an overall design for marine surface vessels that enables safe formation control by a separation between the coordination tasks and the mission task is the main contribution of this work. By controlling points that are offset from the vessels and using a special case of the framework

C.F.L. Thorvaldsen and R. Skjetne are with the Department of Marine Technology, Norwegian University of Science and Technology (NTNU), Trondheim, Norway. E-mails: christoffer.thorvaldsen@ntnu.no and skjetne@ieee.org. Research supported by NTNU project "Applied Underwater Robotics Laboratory (AUR-Lab)".

in [2] for group agreement problems, the design circumvents the problem with local minima in a formation constraint function. The paper also shows how the common velocity input in [2] can be utilized to ensure path-following for the formation. This is done by a maneuvering design in accordance with [3], with some important modifications to ensure a clear-cut separation between the tasks of establishing the formation and performing path-following.

II. Preliminary background

A. Notations

The Euclidean vector norm of $\mathbf{x}$ is denoted $|\mathbf{x}|$, while $||\mathbf{A}||$ denotes the induced Euclidean norm of the matrix $\mathbf{A}$. For a collection of vectors $\mathbf{x}_i \in \mathbb{R}^{n_i}$,

$$col(\mathbf{x}_1, \mathbf{x}_2, \ldots, \mathbf{x}_k) = [\mathbf{x}_1^\top, \mathbf{x}_2^\top, \ldots, \mathbf{x}_k^\top]^\top \in \mathbb{R}^{\sum_{i=1}^k n_i}.$$

Whenever convenient, $\big|(\mathbf{x}, \mathbf{y})\big|$ denotes the norm of the vector $col(\mathbf{x}, \mathbf{y})$. For a collection of square matrices $\mathbf{A}_i \in \mathbb{R}^{n\times n}$,

$$diag(\mathbf{A}_1, \mathbf{A}_2, \ldots, \mathbf{A}_k) \quad \in \mathbb{R}^{kn\times kn}$$

denotes a block diagonal matrix. The smallest and largest eigenvalues of the symmetric positive definite matrix $\mathbf{Q}$ are denoted $\lambda_{min,Q}, \lambda_{max,Q}$. Total time derivatives are denoted by $\dot{\mathbf{f}}, \ddot{\mathbf{f}}$, etc. Partial derivatives of a function $\mathbf{f}(x, y, t)$ are denoted by a superscript $\mathbf{f}^{x^n}(x, y, t) = \frac{\partial^n \mathbf{f}(x,y,t)}{\partial x^n}$, etc. For a scalar multivariable function $f(\mathbf{x})$, we denote $\frac{\partial f(\mathbf{x})}{\partial \mathbf{x}} = col\left(\frac{\partial f(\mathbf{x})}{\partial x_1}, \ldots, \frac{\partial f(\mathbf{x})}{\partial x_n}\right)$. For Kronecker products, see [2] for details, but note the following properties,

$$(\mathbf{A}\otimes\mathbf{B})^\top = \mathbf{A}^\top \otimes \mathbf{B}^\top$$
$$(\mathbf{A}\otimes\mathbf{I}_p)(\mathbf{C}\otimes\mathbf{I}_p) = (\mathbf{AC})\otimes\mathbf{I}_p,$$

where $\mathbf{I}_p \in \mathbb{R}^{p\times p}$ is the identity matrix, and $\mathbf{C}$ is assumed to be compatible for multiplication with $\mathbf{A}$.

B. Vessel models

The following three degree-of-freedom model for marine surface vessels is assumed (see e.g. [1]):

$$\dot{\boldsymbol{\eta}}_i = \mathbf{R}(\psi_i)\boldsymbol{\nu}_i \tag{1a}$$
$$\mathbf{M}_i\dot{\boldsymbol{\nu}}_i + \mathbf{D}_i(\boldsymbol{\nu}_i)\boldsymbol{\nu}_i + \mathbf{C}_i(\boldsymbol{\nu}_i)\boldsymbol{\nu}_i = \boldsymbol{\tau}_i, \tag{1b}$$

Here, $\boldsymbol{\eta}_i = col(x_i, y_i, \psi_i)$ represents the earth-fixed position and orientation of the i'th vessel, $\boldsymbol{\nu}_i = col(u_i, v_i, r_i)$ contains the body-fixed velocity components in surge, sway, and yaw, and $\boldsymbol{\tau}_i$ is the control input. The mass matrix $\mathbf{M}_i$ is assumed to be constant, positive definite and symmetric (although this is not always the case at forward speed due to added mass effects). The matrices $\mathbf{C}_i(\boldsymbol{\nu}_i) = -\mathbf{C}_i(\boldsymbol{\nu}_i)^\top$, $\mathbf{D}_i(\boldsymbol{\nu}_i) > 0$ are the centripetal/Coriolis and damping matrices, respectively, while $\mathbf{R}(\psi) \in \mathcal{SO}(3)$ is the rotation matrix,

$$\mathbf{R}(\psi) = \begin{bmatrix} \cos(\psi) & -\sin(\psi) & 0 \\ \sin(\psi) & \cos(\psi) & 0 \\ 0 & 0 & 1 \end{bmatrix},$$

C. Communication topology

A graph is used to describe the lines of communication between the vessels. Each vessel is a node in the graph, and two vessels can exchange state information if an edge (link) exists between them. For convenience, each link is assigned a direction by letting one of the connected nodes be the negative end and the other the positive end. All communication, however, is assumed bidirectional. For a group of r vessels with p communication links, the graph is represented by the incidence matrix $\mathbf{B} = \{b_{ij}\} \in \mathbb{R}^{r\times p}$, where

$$b_{ij} = \begin{cases} \pm 1 & \text{if the } i\text{'th node is the positive/negative} \\ & \text{end of the } j\text{'th link} \\ 0 & \text{otherwise} \end{cases} \tag{2}$$

Assumption 1: The communication graph is connected at all times, and it does not contain any cycles. Moreover, there exists at most one edge between any given pair of vertices.

A necessary condition for this assumption to be satisfied is that the minimum number of links for r vessels is $p = r-1$. A consequence of the assumption is that the range space of $\mathbf{B}^\top$ spans $\mathbb{R}^p$.

III. Control objective

Consider a group of r vessels to be controlled in formation. To achieve this involves two tasks, a *group coordination* task and a *formation mission* task. The primary task of group coordination is achieved when all the vessels are located at their specified relative position, with a specified relative heading angle, in a local coordinate frame termed the *Formation Reference Frame* $\mathcal{F}$ (see [3]). The secondary objective, the formation mission task, is for the formation as a whole to execute its operational objective. In this paper this is to perform *path-following* along a prespecified smooth path.

A. Setup

Let each vessel in the formation be identified by a unique identifier in the index set $\mathcal{I} = \{1, \ldots, r\}$. The configuration of each vessel i in the formation is given by a possibly time-varying *configuration vector* in $\mathcal{F}$, denoted $\mathbf{l}_i(t) := col(x_{ci}(t), y_{ci}(t), \psi_{ci}(t))$. One can then associate with each vessel an individual Formation Reference Frame $\mathcal{F}_i$, with origin and orientation in the Earth-fixed frame given by

$$\mathbf{x}_{\mathbf{0}i} := \boldsymbol{\eta}_i - \mathbf{R}\left(\psi_i - \psi_{ci}(t)\right)\mathbf{l}_i(t), \tag{3}$$

where $\mathbf{x}_{\mathbf{0}i} = col(x_{0i}, y_{0i}, \psi_{0i})$ is denoted the *Formation Reference Point* (FRP) for Vessel i. Group coordination is then achieved if all $\mathcal{F}_i$, $i \in \mathcal{I}$, are synchronized into a common $\mathcal{F}$, that is, if $\mathbf{x}_{\mathbf{0}1} = \mathbf{x}_{\mathbf{0}2} = \ldots = \mathbf{x}_{\mathbf{0}r}$.

Assumption 2: The configuration vectors $\mathbf{l}_i(t) \in \mathcal{C}^2$, and $\exists\ l_{max} < \infty$ so that $\forall i \in \mathcal{I}$ and $\forall t \geq t_0$, then $\max\{|\mathbf{l}_i(t)|, |\dot{\mathbf{l}}_i(t)|\} \leq l_{max}$.

To address the formation mission task, the strategy is that one vessel, which we will denote as the *acting leader* of the formation, will ensure path-following. When all vessels are coordinated, this will indirectly ensure that the formation as

a whole executes its path-following mission. The choice of acting leader does not have any structural implications on the control system, and it can reassigned to other vessels during a mission. Without loss of generality we let Vessel 1 denote the acting leader, and we target path-following as a *maneuvering problem* [3] involving a geometric task and a dynamic task.

The path-following geometric task is for the FRP of the acting leader to converge to and follow the desired curve given by the set of points

$$\mathcal{P} = \{\boldsymbol{x} \in \mathbb{R}^3 : \exists \theta \text{ s.t. } \mathbf{x} = \mathbf{p}_d(\theta)\}, \tag{4}$$

where $\mathbf{p}_d(\theta) := col(x_d(\theta), y_d(\theta), \psi_d(\theta))$, with $(x_d(\cdot), y_d(\cdot))$ sufficiently smooth functions parameterized by the scalar variable θ, and

$$\psi_d(\theta) = \arctan\left(\frac{y_d^\theta(\theta)}{x_d^\theta(\theta)}\right) \tag{5}$$

chosen as the direction of the tangential vector to the path in each point $(x_d(\theta), y_d(\theta))$.

The dynamic task is represented by a desired speed assignment $v_s(\theta, t)$ for $\dot{\theta}$, which typically is designed to set up a desired speed in [m/s] for the formation along the path [3].

Assumption 3: The path $\mathbf{p}_d(\theta) \in \mathcal{C}^2$, and the speed assignment $v_s(\theta, t) \in \mathcal{C}^1$. There exists $d < \infty$ so that $\forall \theta \in \mathbb{R}$ and $\forall t \geq t_0$, then $\max\{|\mathbf{p}_d^\theta(\theta)|, |v_s(\theta, t)|\} \leq d$.

B. Problem statement

The formation control problem can now be formally stated by the following two objectives:

Group coordination objective: To develop synchronization control laws to ensure that

$$\lim_{t\to\infty} |\mathbf{x}_{\mathbf{0}i}(t) - \mathbf{x}_{\mathbf{0}j}(t)| = 0 \quad \forall i, j \in \mathcal{I}. \tag{6}$$

Formation mission objective: To develop a maneuvering control law to ensure that

$$\lim_{t\to\infty} |\mathbf{x}_{\mathbf{0}1}(t) - \mathbf{p}_d(\theta(t))| = 0, \tag{7}$$

$$\lim_{t\to\infty} |\dot{\theta}(t) - v_s(\theta(t), t)| = 0. \tag{8}$$

The coordination objective is of primary concern and should be achieved before the mission objective is pursued. The reason for this is that having the vessels in formation is a measure for avoiding inter-vessel collisions, especially during the transients when converging to the path. Note, however, that the task of anti-collision is not explicitly targeted in this design.

IV. Control design

A. Group coordination task

In order to design control laws to achieve group coordination, the passivity-based group agreement protocols presented in [2] are used. For the vessels with dynamics (1) and outputs (3), the protocols are used to achieve (6) and

$$\lim_{t\to\infty} |\dot{\mathbf{x}}_{\mathbf{0}i}(t) - \mathbf{v}_d(t)| = 0 \quad \forall i \in \mathcal{I}, \tag{9}$$

where $\mathbf{v}_d(t)$ is a common velocity input to all vessels that later will be used as a degree-of-freedom to solve the formation mission task.

1) Establishing passivity: Motivated by the outline in [2], the first step is to construct partial control laws that transform the vessel dynamics (1) to strictly state passive dynamic systems from auxiliary control inputs $\boldsymbol{\alpha}_i$ to the outputs

$$\boldsymbol{\zeta}_i := \mathbf{R}(\psi_i)^\top (\dot{\mathbf{x}}_{\mathbf{0}i} - \mathbf{v}_d) \quad i \in \mathcal{I}. \tag{10}$$

Using (3), defining $\mathbf{f}_{1i}(\boldsymbol{\eta}_i, t) := \mathbf{R}(\psi_i - \psi_{ci}(t))\,\mathbf{l}_i(t)$ and $\mathbf{f}_{2i}(\boldsymbol{\eta}_i, \boldsymbol{\nu}_i, \mathbf{v}_d, t) := \mathbf{R}(\psi_i)^\top(\dot{\mathbf{f}}_{1i} + \mathbf{v}_d)$, then $\boldsymbol{\zeta}_i$ can be alternatively expressed as

$$\boldsymbol{\zeta}_i = \boldsymbol{\nu}_i - \mathbf{f}_{2i},$$

yielding the dynamics

$$\mathbf{M}_i\dot{\boldsymbol{\zeta}}_i = \boldsymbol{\tau}_i - \mathbf{D}_i(\boldsymbol{\nu}_i)\,(\boldsymbol{\zeta}_i + \mathbf{f}_{2i}) - \mathbf{C}_i(\boldsymbol{\nu}_i)\,(\boldsymbol{\zeta}_i + \mathbf{f}_{2i}) - \mathbf{M}_i\dot{\mathbf{f}}_{2i}$$

Selecting matrices $\mathbf{K}_{\mathbf{d}i} = \mathbf{K}_{\mathbf{d}i}^\top > 0$ and choosing the control inputs as

$$\boldsymbol{\tau}_i = \mathbf{D}_i(\boldsymbol{\nu}_i)\mathbf{f}_{2i} + \mathbf{C}_i(\boldsymbol{\nu}_i)\mathbf{f}_{2i} + \mathbf{M}_i\dot{\mathbf{f}}_{2i} - \mathbf{K}_{\mathbf{d}i}\boldsymbol{\zeta}_i + \boldsymbol{\alpha}_i, \tag{11}$$

yield

$$\mathbf{M}_i\dot{\boldsymbol{\zeta}}_i = -\left(\mathbf{C}_i(\boldsymbol{\nu}_i) + \mathbf{D}_i(\boldsymbol{\nu}_i) + \mathbf{K}_{\mathbf{d}i}\right)\boldsymbol{\zeta}_i + \boldsymbol{\alpha}_i, \tag{12}$$

which is passive from $\boldsymbol{\alpha}_i$ to $\boldsymbol{\zeta}_i$. To show this, the following positive definite, radially unbounded functions are utilized:

$$S_{\zeta i}(\boldsymbol{\zeta}_i) := \frac{1}{2}\boldsymbol{\zeta}_i^\top\mathbf{M}_i\boldsymbol{\zeta}_i \tag{13}$$

Taking time derivatives and using the properties of the $\mathbf{C}_i$ and $\mathbf{D}_i$ matrices yields

$$\begin{aligned}\dot{S}_{\zeta i} &= \boldsymbol{\zeta}_i^\top\mathbf{M}_i\dot{\boldsymbol{\zeta}}_i \\ &= \boldsymbol{\zeta}_i^\top\left(-\mathbf{D}_i(\boldsymbol{\nu}_i)\boldsymbol{\zeta}_i - \mathbf{K}_{\mathbf{d}i}\boldsymbol{\zeta}_i - \mathbf{C}_i(\boldsymbol{\nu}_i)\boldsymbol{\zeta}_i + \boldsymbol{\alpha}_i\right) \\ &\leq -\boldsymbol{\zeta}_i^\top\mathbf{K}_{\mathbf{d}i}\boldsymbol{\zeta}_i + \boldsymbol{\zeta}_i^\top\boldsymbol{\alpha}_i,\end{aligned}$$

which by standard passivity theorems (see [7]) gives the desired result.

2) Synchronization: To complete the first part of the control design, we need to specify the auxiliary control inputs $\boldsymbol{\alpha}_i$. These functions will enable the vessels to synchronize in the limit. Motivated by [2], the functions are chosen as

$$\boldsymbol{\alpha}_i = -\mathbf{R}(\psi_i)^\top\left(\sum_{k=1}^{p} b_{ik}\boldsymbol{\gamma}_k(\mathbf{z}_k)\right) \quad i \in \mathcal{I}, \tag{14}$$

where $\mathbf{B} = \{b_{ij}\} \in \mathbb{R}^{r\times p}$ is the incidence matrix of the communication graph[1]. For the k'th link connecting vessels with indexes i and j, $\mathbf{z}_k$ is the synchronization error between the vessels corresponding to

$$\mathbf{z}_k := \sum_{i=1}^{r} b_{ik}\mathbf{x}_{\mathbf{0}i} = \begin{cases} \mathbf{x}_{\mathbf{0}i} - \mathbf{x}_{\mathbf{0}j} & \text{if } i \text{ is the positive end} \\ \mathbf{x}_{\mathbf{0}j} - \mathbf{x}_{\mathbf{0}i} & \text{if } i \text{ is the negative end} \end{cases} \tag{15}$$

[1]According to Assumption 1 in Section II-C, the number of columns in $\mathbf{B}$ must be $p = r - 1$.

Furthermore, we define

$$\boldsymbol{\gamma}_k(\mathbf{z}_k) := \frac{\partial P_k(\mathbf{z}_k)}{\partial \mathbf{z}_k}, \tag{16}$$

where according to [2], the functions $P_k(\mathbf{z}_k)$ satisfy:

$$P_k \in C^2 \tag{17a}$$
$$P_k(\mathbf{0}) = 0 \tag{17b}$$
$$P_k(\mathbf{z}_k) > 0 \quad \forall \mathbf{z}_k \neq \mathbf{0} \tag{17c}$$
$$P_k(\mathbf{z}_k) \to \infty \text{ as } |\mathbf{z}_k| \to \infty \tag{17d}$$
$$\mathbf{z}_k^\top \frac{\partial P_k(\mathbf{z}_k)}{\partial \mathbf{z}_k} > 0 \quad \forall \mathbf{z}_k \neq \mathbf{0}. \tag{17e}$$

Examining (14) shows that the synchronizing control input for each vessel consists of feedback from the synchronization errors between the vessel and its "neighbors" in the communication topology. The synchronization design thus necessitates only limited inter-vessel communication, corresponding to a decentralized solution. It is noted that since $\mathbf{z}_k$ is required by the control systems of both vessels connected to the k'th link, communication topologies corresponding to unidirectional communication between nodes are not applicable to this design.

B. Formation mission task

Define $\mathbf{q}$ as the path-following error between the FRP of the acting leader and its desired position $\mathbf{p}_d(\theta)$ on the path:

$$\mathbf{q}(\mathbf{x_{01}}, \theta) := \mathbf{x_{01}} - \mathbf{p}_d(\theta), \quad \mathbf{q} \in \mathbb{R}^3. \tag{18}$$

Since $\dot{\mathbf{x}}_{\mathbf{01}} = \mathbf{R}(\psi_1)\boldsymbol{\zeta}_1 + \mathbf{v}_d$, the dynamics of $\mathbf{q}$ becomes

$$\dot{\mathbf{q}} = \mathbf{v}_d - \mathbf{p}_d^\theta(\theta)\dot{\theta} + \mathbf{R}(\psi_1)\boldsymbol{\zeta}_1,$$

where $\boldsymbol{\zeta}_1$ is the synchronization velocity error (10) for the acting leader. In the next step we design control laws for $\mathbf{v}_d$ and $\dot{\theta}$ in order to solve (7) and (8) based on the principle of certainty equivalence $\boldsymbol{\zeta}_1 = \mathbf{0}$.

1) Maneuvering control design: To stabilize $\{\mathbf{q} = 0\}$ we select a Hurwitz matrix $\mathbf{A} \in \mathbb{R}^{3\times 3}$ together with $\mathbf{P} = \mathbf{P}^\top > \mathbf{0}$ satisfying $\mathbf{PA} + \mathbf{A}^\top\mathbf{P} = -\mathbf{Q}$ for a given $\mathbf{Q} = \mathbf{Q}^\top > 0$, and consider the CLF

$$V_q(\mathbf{x_{01}}, \theta) = \mathbf{q}(\mathbf{x_{01}}, \theta)^\top \mathbf{P}\mathbf{q}(\mathbf{x_{01}}, \theta). \tag{19}$$

A simple choice for $\mathbf{v}_d$ and $\dot{\theta}$ is

$$\begin{aligned} \mathbf{v}_d &= \mathbf{A}\mathbf{q}(\mathbf{x_{01}}, \theta) + \mathbf{p}_d^\theta(\theta) v_s(\theta, t), \\ \dot{\theta} &= v_s(\theta, t). \end{aligned} \tag{20}$$

This choice stabilizes the path-following error $\{\mathbf{q} = 0\}$ through $\dot{\mathbf{q}} = \mathbf{Aq}$ (also verified by $\dot{V}_q = -\mathbf{q}^\top\mathbf{Qq}$) for $\boldsymbol{\zeta}_1 = \mathbf{0}$. Additionally, it satisfies the speed assignment along the path (8) identically. However, the above control law has some flaws. Note first that $v_d = v_d(t)$ becomes a velocity command signal which must be broadcasted to all vessels. The most notable flaw is then that the vessels will receive a commanded velocity that drives them towards the path, irrespective of how well they are coordinated.

To remedy this problem and ensure that coordination is handled with higher priority than path-following, the right-hand side terms of (20) will be weighted by *activation functions* that map the synchronization errors into scalar weight signals. These signals should be small for large synchronization errors and equal to unity when synchronized, effectively meaning that the vessels will forget the path while synchronizing. To this end, the functions $\sigma_k : \mathbb{R}_{\geq 0} \mapsto \mathbb{R}_{>0}$ are introduced, which should be $\mathcal{C}^1$, monotonically decreasing, and satisfy

$$\sigma_k(0) = 1 \tag{21a}$$
$$\lim_{s\to\infty} \sigma_k(s) = 0. \tag{21b}$$

As input to these functions, we use $|\mathbf{z}|_L^2 := \mathbf{z}^\top\mathbf{L}\mathbf{z}$, where $\mathbf{z} = col(\mathbf{z}_1, \ldots, \mathbf{z}_p)$, $\mathbf{z} \in \mathbb{R}^{3p}$, and $\mathbf{L} = \mathbf{L}^\top \geq 0$ is a weight matrix used to tune the gains for position and orientation errors[2] in $\mathbf{z}$.

With the activation functions defined, we assign the dynamic control law

$$\mathbf{v}_d = \sigma_1(|\mathbf{z}|_L^2)\mathbf{A}\mathbf{q}(\mathbf{x_{01}}, \theta) + \sigma_2(|\mathbf{z}|_L^2)\mathbf{p}_d^\theta(\theta) v_s(\theta, t) \tag{22}$$
$$\dot{\theta} = \sigma_2(|\mathbf{z}|_L^2) v_s(\theta, t) - \omega, \tag{23}$$

where ω is a free input used to shape the transient in the path convergence phase. In the path-error $\mathbf{q}$, the closed-loop dynamics become

$$\dot{\mathbf{q}} = \sigma_1(|\mathbf{z}|_L^2)\mathbf{A}\mathbf{q} + \mathbf{p}_d^\theta(\theta)\omega + \mathbf{R}(\psi_1)\boldsymbol{\zeta}_1. \tag{24}$$

Motivated by the gradient optimization designs in [3], we assign ω as

$$\omega = \mu(\theta) V_q^\theta(\mathbf{x_{01}}, \theta) = -2\mu(\theta)\mathbf{q}(\mathbf{x_{01}}, \theta)^\top \mathbf{P}\mathbf{p}_d^\theta(\theta), \tag{25}$$

where in contrast to [3], $\mu(\theta) > 0$ is designed as a function of θ to allow normalization with respect to path parameterization. This ensures that the speed of the gradient minimization is independent of how a certain path is parameterized; see Section VI for an example.

Assumption 4: The gain $\mu(\theta) \in \mathcal{C}^1$, and $\exists \mu_{max} < \infty$ so that $\forall \theta \in \mathbb{R}$, then $0 < \mu(\theta) \leq \mu_{max}$.

Differentiating (19) with respect to time yields

$$\begin{aligned} \dot{V}_q &= -\sigma_1(|\mathbf{z}|_L^2)\mathbf{q}^\top\mathbf{Q}\mathbf{q} + 2\mathbf{q}^\top\mathbf{P}\mathbf{p}_d^\theta(\theta)\omega + 2\mathbf{q}^\top\mathbf{P}\mathbf{R}(\psi_1)\boldsymbol{\zeta}_1 \\ &= -\sigma_1(|\mathbf{z}|_L^2)\mathbf{q}^\top\mathbf{Q}\mathbf{q} - \mu(\theta) V_q^\theta(\mathbf{x_{01}}, \theta)^2 + 2\mathbf{q}^\top\mathbf{P}\mathbf{R}(\psi_1)\boldsymbol{\zeta}_1 \\ &\leq -\sigma_1(|\mathbf{z}|_L^2)\mathbf{q}^\top\mathbf{Q}\mathbf{q} + 2\mathbf{q}^\top\mathbf{P}\mathbf{R}(\psi_1)\boldsymbol{\zeta}_1 \end{aligned} \tag{26}$$

For $\mathbf{z}$ confined to compact sets by the control design for group coordination, it follows for $\boldsymbol{\zeta}_1 = \mathbf{0}$ that (7) is satisfied by (18). Furthermore, (8) is satisfied as $\mathbf{z}(t) \to \mathbf{0}$. A detailed analysis of stability for the complete closed-loop system is provided in Section V.

[2]The gains should be selected to normalize the effect of position and orientation errors in $|\mathbf{z}|_L^2$. They can also be used to limit the inter-vessel communication requirements of the control system (see Section VII).

C. Operation phases

The activation functions $\sigma_k(\cdot)$ and the gradient optimization term in $\dot{\theta}$ were introduced to enable the desired priority levels between the group coordination and the formation mission objectives, resulting in an operation effectively divided into a coordination phase and a path-following phase.

1) Coordination phase: In the beginning of an operation, the synchronization errors are typically large. By proper design, the functions $\sigma_1(|\mathbf{z}|_L^2)$ and $\sigma_2(|\mathbf{z}|_L^2)$ can attain arbitrarily small values for $|\mathbf{z}|_{\mathbf{L}} \geq c$, where c is a specified threshold value. This ensures that the common velocity command signal (22) is close to zero when the synchronization errors are large. The result is a low-speed coordination phase where the vessels position themselves relatively to the group without paying any attention to the path-following objective. During this phase, the dynamics of θ is approximately reduced to

$$\dot{\theta} \approx -\mu(\theta) V_q^{\theta}(\mathbf{x_{0}}_1, \theta),$$

which shows that the point $\mathbf{p}_d(\theta(t))$ will move to a favorable position along the path by minimizing $\theta \mapsto V_q(\mathbf{x_{0}}_1, \theta)$, and wait there until the formation is established.

2) Path-following phase: After the group of vessels is sufficiently coordinated, the path-following phase is initiated by a collective movement towards the path. This is a result of the functions $\sigma_1(|\mathbf{z}|_L^2)$ and $\sigma_2(|\mathbf{z}|_L^2)$ now approaching unity, thereby activating the maneuvering feedback and feedforward terms in the common velocity command signal. This also activates the speed assignment $v_s(\theta, t)$ in (23), which drives the desired position and heading $\mathbf{p}_d(\theta(t))$ along the path at the desired speed[3].

V. Stability analysis

A. Preliminary definitions and properties

Define

$$\mathbf{x_0} := col(\mathbf{x_{0}}_1, \ldots, \mathbf{x_{0}}_r) \quad \in \mathbb{R}^{3r} \tag{27}$$
$$\boldsymbol{\psi} := col(\psi_1, \ldots, \psi_r) \quad \in \mathbb{R}^{r} \tag{28}$$
$$\bar{\boldsymbol{\nu}} := col(\boldsymbol{\nu}_1, \ldots, \boldsymbol{\nu}_r) \quad \in \mathbb{R}^{3r} \tag{29}$$
$$\bar{\mathbf{R}}(\boldsymbol{\psi}) := diag\left(\mathbf{R}(\psi_1), \ldots, \mathbf{R}(\psi_r)\right) \quad \in \mathbb{R}^{3r\times 3r} \tag{30}$$
$$\boldsymbol{\alpha}(\mathbf{z}, \boldsymbol{\psi}) := col\left(\boldsymbol{\alpha}_1(\mathbf{z}, \psi_1), \ldots, \boldsymbol{\alpha}_r(\mathbf{z}, \psi_r)\right) \quad \in \mathbb{R}^{3r} \tag{31}$$
$$\boldsymbol{\gamma}(\mathbf{z}) := col(\boldsymbol{\gamma}_1(\mathbf{z}_1), \ldots, \boldsymbol{\gamma}_p(\mathbf{z}_p)) \quad \in \mathbb{R}^{3p} \tag{32}$$
$$\boldsymbol{\zeta} := col(\boldsymbol{\zeta}_1, \ldots, \boldsymbol{\zeta}_r) \quad \in \mathbb{R}^{3r} \tag{33}$$
$$\Upsilon := \mathbf{1}_r \otimes \mathbf{v_d} \quad \in \mathbb{R}^{3r}, \tag{34}$$

where, $\mathbf{1}_r \in \mathbb{R}^r$ is the vector of ones. From the definition of $\boldsymbol{\zeta}_i$ and equations (14), (15), it is verified that the vectors $\mathbf{x_0}$, $\mathbf{z}$, and $\boldsymbol{\alpha}$ satisfy

$$\dot{\mathbf{x}}_{\mathbf{0}} = \bar{\mathbf{R}}(\boldsymbol{\psi})\boldsymbol{\zeta} + \Upsilon \tag{35}$$
$$\mathbf{z} = (\mathbf{B}^{\top} \otimes \mathbf{I}_3)\mathbf{x_0}, \tag{36}$$
$$\boldsymbol{\alpha}(\mathbf{z}, \boldsymbol{\psi}) = -\bar{\mathbf{R}}(\boldsymbol{\psi})^{\top}(\mathbf{B} \otimes \mathbf{I}_3)\boldsymbol{\gamma}(\mathbf{z}), \tag{37}$$

[3]It is also possible to scale $v_s(\theta, t)$ by a third weight function $\sigma_3(|\mathbf{q}|_{L_2}^2)$, to ensure that the speed assignment is not activated before the FRP of the acting leader has converged to the path, i.e. $\mathbf{q} \approx 0$.

where $\mathbf{I}_3 \in \mathbb{R}^{3\times 3}$ is the identity matrix. Furthermore, since the sum of entries in any column of $\mathbf{B}$ is equal to zero, the basis for the nullspace $\mathcal{N}(\mathbf{B}^{\top} \otimes \mathbf{I}_3)$ is

$$\left\{\mathbf{u} \in \mathbb{R}^{3r} : \mathbf{u} = \mathbf{1}_r \otimes \mathbf{c}, \quad \mathbf{c} \in \mathbb{R}^3\right\}, \tag{38}$$

from which it follows

$$(\mathbf{B}^{\top} \otimes \mathbf{I}_3)\Upsilon = \mathbf{0}. \tag{39}$$

A consequence of the connectivity assumption on the communication graph is the following lemma:

Lemma 1: For a connected communication graph with r nodes, p edges and index set $\mathcal{I}$, then $\forall i, j \in \mathcal{I}$ there exists $\mathbf{K}_{ij} = [a_1\mathbf{I}_3, a_2\mathbf{I}_3, \ldots, a_p\mathbf{I}_3] \in \mathbb{R}^{3\times 3p}$, with $a_l \in \{-1, 0, 1\}$, $l = 1 \ldots p$, such that

$$\mathbf{x_{0}}_i - \mathbf{x_{0}}_j = \mathbf{K}_{ij}\mathbf{z}.$$

It follows from this lemma that $\mathbf{z} = \mathbf{0}$ solves the coordination objective (6).

B. Closed-loop system

The total closed-loop dynamics become

$$\mathbf{M}_i\dot{\boldsymbol{\zeta}}_i = -\left(\mathbf{C}_i(\boldsymbol{\nu}_i) + \mathbf{D}_i(\boldsymbol{\nu}_i) + \mathbf{K_d}_i\right)\boldsymbol{\zeta}_i + \boldsymbol{\alpha}_i(\mathbf{z}, \psi_i), i \in \mathcal{I} \tag{40}$$
$$\dot{\mathbf{z}} = (\mathbf{B}^{\top} \otimes \mathbf{I}_3)\bar{\mathbf{R}}(\boldsymbol{\psi})\boldsymbol{\zeta} \tag{41}$$
$$\dot{\mathbf{q}} = \sigma_1(|\mathbf{z}|_{L_1}^2)\mathbf{A}\mathbf{q} - 2\mu(\theta)\mathbf{p}_d^{\theta}(\theta)\mathbf{q}^{\top}\mathbf{P}\mathbf{p}_d^{\theta}(\theta) + \mathbf{R}(\psi_1)\boldsymbol{\zeta}_1 \tag{42}$$
$$\dot{\theta} = \sigma_2(|\mathbf{z}|_{L_1}^2)v_s(\theta, t) + 2\mu(\theta)\mathbf{q}^{\top}\mathbf{P}\mathbf{p}_d^{\theta}(\theta). \tag{43}$$

It can be verified that $\psi_i = \psi_{0i} + \psi_{ci}(t)$, where $\psi_{0i} = \mathbf{e}^{\top}\left(\mathbf{K}_{i1}\mathbf{z} + \mathbf{q} + \mathbf{p}_d(\theta)\right)$, $\mathbf{e} = col(0, 0, 1)$, and that

$$\boldsymbol{\nu}_i = \mathbf{H}(t)\Big(\boldsymbol{\zeta}_i + \mathbf{R}(\psi_i)^{\top}\mathbf{v}_d + \mathbf{R}(\psi_{ci}(t))^{\top}\left(\dot{\mathbf{l}}_i(t) - \mathbf{S}\mathbf{l}_i(t)\dot{\psi}_{ci}(t)\right)\Big), \tag{44}$$

where

$$\begin{aligned}\mathbf{H}(t) &= (\mathbf{I}_3 - \mathbf{R}(\psi_{ci}(t))^{\top}\mathbf{S}\mathbf{l}_i(t)\mathbf{e}^{\top})^{-1} \\ &= (\mathbf{I}_3 + \mathbf{R}(\psi_{ci}(t))^{\top}\mathbf{S}\mathbf{l}_i(t)\mathbf{e}^{\top}),\end{aligned}$$

and $\mathbf{S}$ is the skew-symmetric matrix satisfying $\frac{\partial \mathbf{R}(\psi)}{\partial \psi} = \mathbf{R}(\psi)\mathbf{S}$. By defining

$$\boldsymbol{\chi} := col(\mathbf{z}, \boldsymbol{\zeta}, \mathbf{q}) \quad \in \mathbb{R}^{3(p+r+1)}, \tag{45}$$

we can thus write the closed-loop dynamics compactly as

$$\begin{bmatrix}\dot{\boldsymbol{\chi}} \\ \dot{\theta}\end{bmatrix} = \begin{bmatrix}\mathbf{f}_{\chi}(t, \boldsymbol{\chi}, \theta) \\ f_{\theta}(t, \boldsymbol{\chi}, \theta)\end{bmatrix} =: \mathbf{F}(t, \boldsymbol{\chi}, \theta). \tag{46}$$

Note that in general, the closed-loop error dynamics are valid for $(\mathbf{z}, \boldsymbol{\zeta}, \mathbf{q}, \theta) \in \{\mathcal{R}\big((\mathbf{B}^{\top} \otimes \mathbf{I}_3)\big) \times \mathbb{R}^{3r} \times \mathbb{R}^3 \times \mathbb{R}\}$. From Assumption 1, however, we have that $\mathcal{R}(\mathbf{B}^{\top}) = \mathbb{R}^p$, which implies that $\mathcal{R}\big((\mathbf{B}^{\top} \otimes \mathbf{I}_3)\big) = \mathbb{R}^{3p}$. This means that the stated closed-loop dynamics are valid over the entire state space, enabling the global stability result given in the following theorem:

Theorem 1: Under assumptions 1 – 4, the control laws (11), (22), (23), and (25) render the closed-loop system (46) forward complete and the set $\{(\boldsymbol{\chi}, \theta, t) : \boldsymbol{\chi} = 0\}$ UGAS. This solves the control objectives (6), (7), and (8).

C. Proof of Theorem 1

1) Forward completeness: Define the function

$$V_{z,\zeta}(\mathbf{z},\boldsymbol{\zeta}) := \sum_{k=1}^{p} P_k(\mathbf{z}_k) + \sum_{i=1}^{r} S_{\zeta_i}(\boldsymbol{\zeta}_i) \tag{47}$$

Since this function is both positive definite and radially unbounded in $(\mathbf{z},\boldsymbol{\zeta})$, by [7, Lemma 4.3] there exists class-$\mathcal{K}_\infty$ functions ϕ_1, ϕ_2 so that

$$\phi_1(|(\mathbf{z},\boldsymbol{\zeta})|) \leq V_{z,\zeta} \leq \phi_2(|(\mathbf{z},\boldsymbol{\zeta})|). \tag{48}$$

Differentiating (47) yields

$$\begin{aligned}
\dot{V}_{z,\zeta} &= \left[\frac{\partial}{\partial \mathbf{z}}\left(\sum_{k=1}^{p} P_k(\mathbf{z}_k)\right)\right]^\top \dot{\mathbf{z}} + \sum_{i=1}^{r} \dot{S}_{\zeta,i} \\
&\leq \boldsymbol{\gamma}(\mathbf{z})^\top (\mathbf{B}^\top \otimes \mathbf{I}_3)\bar{\mathbf{R}}(\boldsymbol{\psi})\boldsymbol{\zeta} + \sum_{i=1}^{r} (-\boldsymbol{\zeta}_i^\top \mathbf{K}_{\mathbf{d}i}\boldsymbol{\zeta}_i + \boldsymbol{\zeta}_i^\top \boldsymbol{\alpha}_i) \\
&= -\boldsymbol{\alpha}^\top \boldsymbol{\zeta} - \sum_{i=1}^{r} (\boldsymbol{\zeta}_i^\top \mathbf{K}_{\mathbf{d}i}\boldsymbol{\zeta}_i) + \boldsymbol{\zeta}^\top \boldsymbol{\alpha} \\
&= -\sum_{i=1}^{r} (\boldsymbol{\zeta}_i^\top \mathbf{K}_{\mathbf{d}i}\boldsymbol{\zeta}_i) \leq 0
\end{aligned} \tag{49}$$

Since $\dot{V}_{z,\zeta} \leq 0$, this implies for all t in the maximum interval of existence $[t_0, T)$, that $V_{z,\zeta}(t) \leq V_{z,\zeta}(t_0)$. Combining this with (48) yields

$$\left|\big(\mathbf{z}(t),\boldsymbol{\zeta}(t)\big)\right| \leq \phi_3\left(\left|\,(\mathbf{z}(t_0),\boldsymbol{\zeta}(t_0))\,\right|\right) \tag{50}$$

where $\phi_3(\cdot) := \phi_1^{-1} \circ \phi_2(\cdot) \in \mathcal{K}_\infty$.

Next, consider the positive definite, radially unbounded function (19) satisfying

$$\lambda_{min,P}|\mathbf{q}|^2 \leq V_q \leq \lambda_{max,P}|\mathbf{q}|^2. \tag{51}$$

On the time interval $[t_0, T)$, the bounds (50) and the fact that $\sigma_1(\cdot)$ is monotonically decreasing give a lower bound on $\sigma_1(|\mathbf{z}(t)|_L^2)$ according to

$$\sigma_1(|\mathbf{z}(t)|_L^2) \geq \sigma_1(||\mathbf{L}||\phi_3\left(\left|\,(\mathbf{z}(t_0),\boldsymbol{\zeta}(t_0))\,\right|\right)^2) =: \epsilon_1. \tag{52}$$

From (26) we then get the following over $[t_0, T)$, noting that $||\mathbf{R}(\psi)|| = 1\ \forall \psi \in \mathbb{R}$:

$$\begin{aligned}
\dot{V}_q &\leq -\epsilon_1 \mathbf{q}^\top \mathbf{Q}\mathbf{q} + 2\mathbf{q}^\top \mathbf{P}\mathbf{R}(\psi_1)\boldsymbol{\zeta}_1 \\
&\leq -\epsilon_1 \lambda_{min,Q}|\mathbf{q}|^2 + 2|\mathbf{q}||\mathbf{P}||\boldsymbol{\zeta}_1| \\
&\leq -\frac{1}{2}\epsilon_1 \lambda_{min,Q}|\mathbf{q}|^2 \quad \forall |\mathbf{q}| \geq \frac{4||\mathbf{P}||}{\epsilon_1 \lambda_{min,Q}}|\boldsymbol{\zeta}_1|
\end{aligned}$$

For

$$|\mathbf{q}| \geq \frac{4||\mathbf{P}||\phi_3\left(\left|\,(\mathbf{z}(t_0),\boldsymbol{\zeta}(t_0))\,\right|\right)}{\epsilon_1 \lambda_{min,Q}} =: \epsilon_2,$$

we are thus guaranteed $\dot{V}_q \leq 0$, which yields

$$\begin{aligned}
V_q(t) &\leq \max\{V_q(\mathbf{q}(t_0)),\ \sup_{|\mathbf{q}|=\epsilon_2} V_q(\mathbf{q})\} \\
&\leq V_q(\mathbf{q}(t_0)) + \sup_{|\mathbf{q}|=\epsilon_2} V_q(\mathbf{q}) \\
&\leq \lambda_{max,P}|\mathbf{q}(t_0)|^2 + \lambda_{max,P}\epsilon_2^2 \quad \forall t \in [t_0, T).
\end{aligned}$$

From this, we finally get uniform upper bounds for $|\mathbf{q}(t)|$ over the time interval $[t_0, T)$:

$$|\mathbf{q}(t)| \leq \sqrt{\frac{\lambda_{max,P}}{\lambda_{min,P}}}\,(|\mathbf{q}(t_0)| + \epsilon_2) \tag{53}$$

Combining this with assumptions 3 and 4, we achieve a uniform upper bound for $|\dot{\theta}|$ over $[t_0, T)$, which shows that there cannot be a finite escape time for the system (46), i.e. $T = +\infty$. By a locally Lipschitz property of the closed-loop system, we conclude that the solutions $\theta(t)$ and $\boldsymbol{\chi}(t)$ exist and are continuous functions over $[t_0, \infty)$.

For the remainder of the analysis, θ will be treated as an external input, continuous in time, that enters the dynamics of $\boldsymbol{\chi}$. Stability of the origin of

$$\dot{\boldsymbol{\chi}} = \mathbf{f}(t, \boldsymbol{\chi}), \tag{54}$$

where $\mathbf{f}(t,\boldsymbol{\chi}) := \mathbf{f}_\chi(t, \boldsymbol{\chi}, \theta(t))$, will be investigated by the means of the Nested Matrosov Theorem for time-varying systems presented in [8].

2) Uniform Global Stability: To apply the Nested Matrosov Theorem, UGS of the origin is first established. By forward completeness of the total closed loop system, the bounds in (50) and (53) hold $\forall t \geq t_0$.

Since $|\boldsymbol{\chi}| \leq |\big(\mathbf{z},\boldsymbol{\zeta}\big)| + |\mathbf{q}|$, $|\boldsymbol{\chi}| \geq |\big(\mathbf{z},\boldsymbol{\zeta}\big)|$, and $|\boldsymbol{\chi}| \geq |\mathbf{q}|$, we have that

$$\begin{aligned}
&|\boldsymbol{\chi}(t)| \leq \phi_3\left(\left|\,(\mathbf{z}(t_0),\boldsymbol{\zeta}(t_0))\,\right|\right) + \\
&\sqrt{\frac{\lambda_{max,P}}{\lambda_{min,P}}}\left[|\mathbf{q}(t_0)| + \frac{4||\mathbf{P}||\phi_3\left(\left|\,(\mathbf{z}(t_0),\boldsymbol{\zeta}(t_0))\,\right|\right)}{\epsilon_1 \lambda_{min,Q}}\right] \\
&\leq \phi_3\left(|\boldsymbol{\chi}(t_0)|\right) + \\
&\sqrt{\frac{\lambda_{max,P}}{\lambda_{min,P}}}\left[|\boldsymbol{\chi}(t_0)| + \frac{4||\mathbf{P}||\phi_3\left(|\boldsymbol{\chi}(t_0)|\right)}{\lambda_{min,Q}\sigma_1\left(||\mathbf{L}||\phi_3\left(|\boldsymbol{\chi}(t_0)|\right)^2\right)}\right] \\
&=: \phi_4(|\boldsymbol{\chi}(t_0)|)
\end{aligned}$$

Since $\phi_3(\cdot) \in \mathcal{K}^\infty$ and $\sigma_1(\cdot)$ is monotonically decreasing and strictly positive, we have that $\phi_4(\cdot) \in \mathcal{K}^\infty$, which shows that the origin is UGS.

3) Uniform Global Asymptotic Stability: Defining

$$V_0(\boldsymbol{\chi}) := V_{z,\zeta}(\mathbf{z},\boldsymbol{\zeta}), \tag{55}$$

we have from (49) that

$$\dot{V}_0 \leq \sum_{i=1}^{r} (-\boldsymbol{\zeta}_i^\top \mathbf{K}_{\mathbf{d}i}\boldsymbol{\zeta}_i) =: Y_0(\boldsymbol{\chi}) \leq 0 \quad \forall \boldsymbol{\chi}, \tag{56}$$

where it is noted that $Y_0(\boldsymbol{\chi}) = 0$ implies $\boldsymbol{\zeta} = \mathbf{0}$. Now, define the first auxiliary function[4]

$$V_1(t,\boldsymbol{\chi}) := \mathbf{z}^\top (\mathbf{B} \otimes \mathbf{I}_3)^\ddagger \bar{\mathbf{R}}(\boldsymbol{\psi})\bar{\mathbf{M}}\boldsymbol{\zeta}, \tag{57}$$

where

$$\bar{\mathbf{M}} := diag(\mathbf{M}_1, \ldots, \mathbf{M}_r) \quad \in \mathbb{R}^{3r \times 3r}, \tag{58}$$

[4]The time dependency of this function comes from $\psi_i = \psi_i(\mathbf{z}, \mathbf{q}, \theta(t), t)$, as shown in Section V-B.

and $(\mathbf{B}\otimes\mathbf{I}_3)^\ddagger \in \mathbb{R}^{3p\times 3r}$ is the Moore-Penrose pseudo-inverse of $(\mathbf{B}\otimes\mathbf{I}_3)$ satisfying

$$(\mathbf{B}\otimes\mathbf{I}_3)(\mathbf{B}\otimes\mathbf{I}_3)^\ddagger(\mathbf{B}\otimes\mathbf{I}_3) = (\mathbf{B}\otimes\mathbf{I}_3)$$

Differentiating (57) with respect to time yields

$$\begin{aligned}\dot{V}_1 &= \boldsymbol{\zeta}^\top\bar{\mathbf{R}}(\boldsymbol{\psi})^\top(\mathbf{B}\otimes\mathbf{I}_3)(\mathbf{B}\otimes\mathbf{I}_3)^\ddagger\bar{\mathbf{R}}(\boldsymbol{\psi})\bar{\mathbf{M}}\boldsymbol{\zeta}\\ &\quad+\mathbf{z}^\top(\mathbf{B}\otimes\mathbf{I}_3)^\ddagger\big(\dot{\bar{\mathbf{R}}}(\boldsymbol{\psi},\bar{\boldsymbol{\nu}})\bar{\mathbf{M}}\boldsymbol{\zeta}+\bar{\mathbf{R}}(\boldsymbol{\psi})\bar{\mathbf{M}}\dot{\boldsymbol{\zeta}}\big)\\ &=: Y_1(\boldsymbol{\chi},\boldsymbol{\phi}(t,\boldsymbol{\chi}))\end{aligned}$$

Here, all time dependent terms of $\dot{V}_1(t,\boldsymbol{\chi})$ have been collected in the vector $\boldsymbol{\phi}(t,\boldsymbol{\chi})$, defined as

$$\boldsymbol{\phi}(t,\boldsymbol{\chi}) := col(\bar{\mathbf{R}}(\boldsymbol{\psi})\boldsymbol{\zeta},\bar{\mathbf{R}}(\boldsymbol{\psi})\bar{\mathbf{M}}\boldsymbol{\zeta},\dot{\bar{\mathbf{R}}}(\boldsymbol{\psi},\bar{\boldsymbol{\nu}})\bar{\mathbf{M}}\boldsymbol{\zeta},\bar{\mathbf{R}}(\boldsymbol{\psi})\bar{\mathbf{M}}\dot{\boldsymbol{\zeta}}) \tag{59}$$

Evaluating $Y_1(\boldsymbol{\chi},\boldsymbol{\phi}(t,\boldsymbol{\chi}))$ at $\boldsymbol{\zeta}=\mathbf{0}$, and using (40) yields:

$$\begin{aligned}Y_1(\boldsymbol{\chi},\boldsymbol{\phi}(t,\boldsymbol{\chi}))\Big|_{\boldsymbol{\zeta}=0} &= \mathbf{z}^\top(\mathbf{B}\otimes\mathbf{I}_3)^\ddagger\bar{\mathbf{R}}(\boldsymbol{\psi})(\bar{\mathbf{M}}\dot{\boldsymbol{\zeta}})\Big|_{\boldsymbol{\zeta}=0}\\ &= \mathbf{z}^\top(\mathbf{B}\otimes\mathbf{I}_3)^\ddagger\bar{\mathbf{R}}(\boldsymbol{\psi})\boldsymbol{\alpha}(\mathbf{z},\boldsymbol{\psi})\\ &= -\mathbf{z}^\top(\mathbf{B}\otimes\mathbf{I}_3)^\ddagger\bar{\mathbf{R}}(\boldsymbol{\psi})\bar{\mathbf{R}}(\boldsymbol{\psi})^\top(\mathbf{B}\otimes\mathbf{I}_3)\boldsymbol{\gamma}(\mathbf{z})\\ &= -\mathbf{x_0}^\top(\mathbf{B}\otimes\mathbf{I}_3)(\mathbf{B}\otimes\mathbf{I}_3)^\ddagger(\mathbf{B}\otimes\mathbf{I}_3)\boldsymbol{\gamma}(\mathbf{z})\\ &= -\mathbf{x_0}^\top(\mathbf{B}\otimes\mathbf{I}_3)\boldsymbol{\gamma}(\mathbf{z})\\ &= -\mathbf{z}^\top\boldsymbol{\gamma}(\mathbf{z}) < 0 \quad \forall\mathbf{z}\neq\mathbf{0}\end{aligned}$$

The last inequality follows from the definition of $\boldsymbol{\gamma}_k(\mathbf{z}_k)$ in (16) and the properties listed in (17). Now, define the second auxiliary function

$$V_2(\boldsymbol{\chi}) := V_q(\mathbf{q}) \tag{60}$$

which satisfies

$$\dot{V}_2 \leq -\sigma_1(|\mathbf{z}|_L^2)\mathbf{q}^\top\mathbf{Q}\mathbf{q} + 2\mathbf{q}^\top\mathbf{P}\mathbf{R}(\psi_1)\boldsymbol{\zeta}_1 =: Y_2(\boldsymbol{\chi},\boldsymbol{\phi}(t,\boldsymbol{\chi})) \tag{61}$$

Evaluating $Y_2(\boldsymbol{\chi},\boldsymbol{\phi}(t,\boldsymbol{\chi}))$ at $\boldsymbol{\zeta},\mathbf{z}=\mathbf{0}$ yields

$$Y_2(\boldsymbol{\chi},\boldsymbol{\phi}(t,\boldsymbol{\chi}))\Big|_{\boldsymbol{\zeta},\mathbf{z}=\mathbf{0}} = -\mathbf{q}^\top\mathbf{Q}\mathbf{q} < 0 \quad \forall\mathbf{q}\neq\mathbf{0}$$

We now have that $Y_0(\boldsymbol{\chi}), Y_1(\boldsymbol{\chi},\boldsymbol{\phi}(t,\boldsymbol{\chi})), Y_2(\boldsymbol{\chi},\boldsymbol{\phi}(t,\boldsymbol{\chi})) = 0$ together imply $\boldsymbol{\chi}=\mathbf{0}$.

By the continuity of $\theta(t)$ and smoothness assumptions on $\mathbf{p}_d(\theta)$, $P_k(\mathbf{z}_k)$, and $\mathbf{l}_i(t)$, it follows from utilization of [7, Lemma 3.2] that the functions $V_i(t,\boldsymbol{\chi})$ are locally Lipschitz over $[t_0,\infty)\times\mathbb{R}^{3(r+p+1)}$. Moreover, it is easily verified that $|V_i(t,\boldsymbol{\chi})|$ are uniformly upper bounded for bounded $|\boldsymbol{\chi}|$. Finally, using the fact that $|\boldsymbol{\nu}_i(t,\boldsymbol{\chi})|$ are uniformly upper bounded for bounded $|\boldsymbol{\chi}|$ (this follows from (44) and assumptions 2 – 3), it is verified that $|\boldsymbol{\phi}(t,\boldsymbol{\chi})|$ is uniformly upper bounded for bounded $|\boldsymbol{\chi}|$. All assumptions of [8, Theorem 1] are satisfied, and UGAS for the origin of (54) is established. By Lemma 1 and the closed-loop dynamics of θ in (43), it follows that the control objectives (6)-(8) are satisfied. □

VI. Simulation

The proposed control-scheme is demonstrated numerically for three ships with dynamics given by (1), where the mass matrices are identical, the damping is given by

$$\mathbf{D}_i(\boldsymbol{\nu}_i) = \mathbf{D}_L + \mathbf{D}_u|u_i| + \mathbf{D}_v|v_i| + \mathbf{D}_r|r_i|, \tag{62}$$

and $\mathbf{C}_i(\boldsymbol{\nu}_i)$ is calculated based on the mass matrix from the procedures in [1]. The numerical values for the involved matrices are

$$\mathbf{M}_i = 10^7\begin{bmatrix}0.027521 & 0 & 0\\ 0 & 0.076348 & -0.073803\\ 0 & -0.073803 & 6.690963\end{bmatrix}$$

$$\mathbf{D}_L = 10^6\begin{bmatrix}0.000025 & 0 & 0\\ 0 & 0.009865 & 0.001375\\ 0 & 0.000711 & 2.813355\end{bmatrix}$$

$$\mathbf{D}_u = 10^6\begin{bmatrix}0.002375 & 0 & 0\\ 0 & 0.008843 & 0\\ 0 & 0.111774 & 6.047978\end{bmatrix}$$

$$\mathbf{D}_v = 10^7\begin{bmatrix}0 & 0 & 0\\ 0 & 0.000283 & 0.013495\\ 0 & 0 & 1.188650\end{bmatrix}$$

$$\mathbf{D}_r = 10^8\times diag(0, 0.009537, 1.562880)$$

The earth-fixed frame gives north-position along its x-axis, and east-position along its y-axis. The parameterized path is chosen as $x_d(\theta) = 100\sin(\frac{\pi}{400}\theta)+100$, $\mathbf{y}_d(\theta) = \theta+100$. The desired formation configuration is chosen as $\mathbf{l}_1 = col(0,80,0)$, $\mathbf{l}_2 = col(0,0,0)$, $\mathbf{l}_3 = col(0,-80,0)$, which corresponds to a transversal line formation where a tangential heading angle is common for all the ships. The communication topology is chosen according to two communication links, where Vessel 1 is the positive end of both links. Vessel 3 is set as the acting leader.

The control-specific parameters are chosen according to $\mathbf{K_d}_i = 10^4\times diag(6.5,6.5,1300)$, $\mathbf{A} = diag(-0.02,-0.02,-0.03)$, $\mathbf{P} = \frac{3}{2}\times10^{-2}\times diag(1,1,10^{-5})$, $\mathbf{L} = diag(\mathbf{L}_0,\mathbf{L}_0)$, $\mathbf{L}_0 = diag(1,1,2500)$. The control-specific functions are chosen according to $P_k(\mathbf{z}_k) = \frac{1}{2}(az_{k1}^2 + az_{k2}^2 + bz_{k3}^2)$, $a=4500, b=6\times10^5$, $\sigma_1(s) = \sigma_2(s) = \exp(-0.25s)$, $v_s(\theta,t) = \frac{3}{\sqrt{x_d^\theta(\theta)^2+y_d^\theta(\theta)^2}}$, $\mu(\theta) = \frac{1}{\sqrt{x_d^\theta(\theta)^2+y_d^\theta(\theta)^2}}$.

The initial positions of the vessels are chosen as $\boldsymbol{\eta}_{10} = col(-70,185,\frac{\pi}{10})$, $\boldsymbol{\eta}_{20} = col(-50,140,0)$, $\boldsymbol{\eta}_{30} = col(-80,50,-\frac{\pi}{6})$, while $\theta_0 = 50$. To illustrate the strong separation achieved between the group coordination and formation mission objectives, a "blackout" is inflicted to Vessel 1 after $t = 550[s]$ (at this point, the east-position of Vessel 1 is $\approx 1200[m]$). The result is that the vessel loses its thrust capabilities ($\boldsymbol{\tau}_1 = \mathbf{0}$), thereby losing speed and drifting off the path.

The simulation results are shown in Fig.1 and Fig.2.

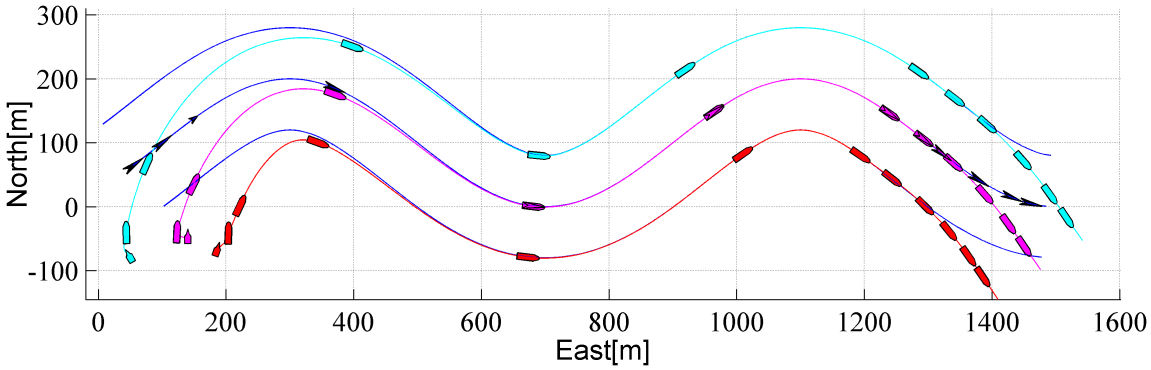

Fig. 1. North-east position plot for the three vessels. The red, purple, and blue ships correspond to vessels 1, 2, and 3, respectively. The black arrowhead on the path indicates the position of $\mathbf{p}_d(\theta)$ which the FRP of the acting leader should converge to. Initial positions are indicated by smaller-sized ships and arrowhead.

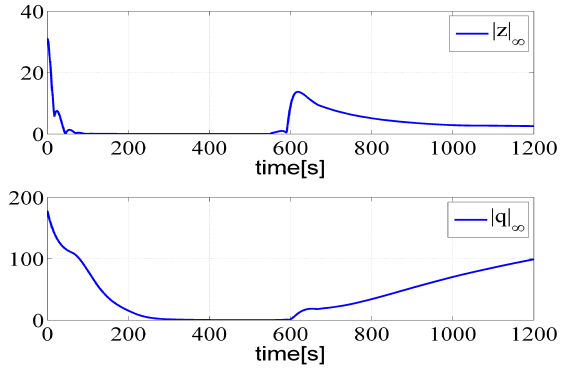

Fig. 2. Time-series of $|\mathbf{z}(t)|_\infty$ and $|\mathbf{q}(t)|_\infty$

It is seen that the vessels synchronize before they initiate movement towards the path. The decrease in $|\mathbf{q}|_\infty$ during synchronization is attributed to the gradient optimization incorporated in the dynamics of θ. After the blackout, the two vessels that still are operational abandon the formation mission objective, concentrating solely on decreasing the synchronization errors by following the drifting vessel. It is seen that steady state synchronization errors arise after the blackout. This is due to Vessel 1 not partaking in the synchronization work. The errors are, however, kept within reasonable limits.

VII. Conclusion

This paper has addressed the topic of formation control for fully actuated marine surface vessels within a path-following framework. Rooted in an operational philosophy where the formation should be maintained at all costs, the design enables strong separation and prioritization between the task of getting the vessels into formation, and the task of getting the formation to follow a prespecified path. This separation provides indirectly some measures for inter-vessel collision avoidance during the path-following phase. However, the design cannot guarantee collision-avoidance during the coordination phase for unfortunate initial conditions.

By following the group agreement protocols in [2], the coordination between the vessels is performed through a decentralized communication topology. However, as path-following requires that each vessel has access to a common velocity signal that is calculated based on the states of all vessels, due to the activation functions, the proposed solution requires global communication between the vessels in general. By choosing the matrix $\mathbf{L}$ such that only the $\mathbf{z}_k$'s that are available locally to the acting leader are required in calculating $|\mathbf{z}|_L^2$, the common velocity input (22) can be generated locally by the acting leader and distributed to the other vessels through the communication topology. This would decentralize the design, but at the same time introduce time-delays. Achieving a fully decentralized design has not been the focus in this paper, but is certainly a topic for future work, in addition to the effect of communication delays on the closed loop performance.

References

[1] Fossen, T. I., *Guidance and Control of Marine Craft*. Draft, 2010.

[2] Arcak, M., Passivity as a design tool for group coordination. *IEEE Transactions on Automatic Control,* 52(8):1381-1390, 2007.

[3] Skjetne, R., *The Maneuvering Problem*. PhD thesis, NTNU, 2005.

[4] Skjetne, R., Ihle, I.-A. F., and Fossen, T. I., *Formation control by synchronizing multiple maneuvering systems*. Proc. IFAC Conf. Maneuvering and Contr. Marine Crafts, NTNU, IFAC, Girona, Spain, pp. 280–285., 2003.

[5] Ihle, I.-A. F., Arcak, M., and Fossen, T. I., Passivity-based designs for synchronized path-following. *Automatica,* 43:1508-1518, 2007.

[6] Breivik, M., Hovstein, V. E. and Fossen, T. I., Ship Formation Control: A Guided Leader-Follower Approach. *Proceedings of the 17th World Congress The International Federation of Automatic Control (IFAC'08), pp. 16008-16014,* 2008, 6-11 July - Seoul, Korea.

[7] Khalil, H. K., *NonLinear Systems*. Prentice Hall, 2002.

[8] Loria, A., Panteley, E., Popovic, D., and Teel, A. R., A nested Matrosov Theorem and Persistency of Excitation for Uniform Convergence in Stable Nonautonomous Systems. *IEEE Transactions on Automatic Control,* 50(2):183-198, 2005.

[9] Bai, H., Arcak, M., and Wen, J. T., Adaptive design for reference velocity recovery in motion coordination. *Systems & control letters,* 57:602-610,2008.

[10] Egerstedt, M. and Hu, X., Formation constrained multi-agent control. *IEEE Transactions on Robotics abd Automation,* 17:947-951, 2001.

[11] Leonard, N. E. and Fiorelli, E., Virtual leaders, artificial potentials and coordinated control of groups. *Proceedings of the 40th IEEE conference on Decision and Control,* pages 2968-2973, 2001.

[12] Lewis, M. A. and Tan, K.-H., High precision formation control of mobile robots using virtual structures. *Autonomous Robots,* 4:387-403, 1997.

[13] Olfati-Saber, R. and Murray, R. M., Distributed cooperative control of multiple vehicle formations using structural potential functions. IFAC World Congress, 2002.

[14] Breivik, M., Subbotin, M. V., and Fossen, T. I., Guided formation control for wheeled mobile robots. *Proceedings of the 9th ICARCV*, 2006.

[15] Grøtli, E. I., Chaillet, A., and Gravdahl, J. T., Output Control of Spacecraft in Leader Follower Formation, *Proceedings of the 47th IEEE Conference on Decision and Control,* 2008

[16] Ren, W., and Beard, R.W., Decentralized scheme for spacecraft formation flying via the virtual structure approach, *Journal of Guidance, Control, and Dynamics,* 27(1), 2004